IOP Publishing Smart Materials and Structures
Smart Mater. Struct. **29** (2020) 085008 (11pp) https://doi.org/10.1088/1361-665X/ab9060

Self-sensing piezoelectric bistable laminates for morphing structures

V S C Chillara, A K Ramanathan and M J Dapino

NSF IUCRC on Smart Vehicle Concepts, Department of Mechanical and Aerospace Engineering, The Ohio State University, Columbus, OH 43210, United States of America

E-mail: chillara.1@osu.edu, ramanathan.38@osu.edu and dapino.1@osu.edu

Received 26 January 2020, revised 19 April 2020
Accepted for publication 5 May 2020
Published 29 June 2020

Abstract

Bistable laminates offer opportunities for shape morphing, energy harvesting, and flow control devices. Smart materials such as piezoelectric macrofiber composites and shape memory alloys have been embedded in bistable laminates to actuate or harvest energy. However, sensor systems capable of measuring bistable shapes and snap-through events are lacking. In this paper, we present curved bistable laminates layered with piezoelectric PVDF films that can sense smooth shape changes as well as abrupt snap-through transitions. Near-static measurement is facilitated by a drift compensated charge amplifier with a large time constant that converts the sensor's charge output into a measurable voltage with minimal drift error. The sensing function is demonstrated on mechanically-prestressed bistable laminates. The laminated composites include two sensor layers such that one measures the changes in curvature and the other measures snap-through events. An analytical model is presented in which strains and curvatures calculated using a laminated-plate model are fed into a linear piezoelectric model to calculate voltage. Shapes measured by the sensors correlate well with shapes measured using a 3D motion capture system. A model-based analysis is performed to understand the laminates' design space.

Keywords: bistable, morphing, analytical model, sensing, piezoelectric PVDF

(Some figures may appear in colour only in the online journal)

1. Introduction

Bistable laminated composites are attractive for morphing structures because they can hold deformed stable shapes and require actuation only to switch between shapes. Bistable elements in a structure have been demonstrated as airflow control devices such as NACA air ducts [1], air intake systems [2], and morphing winglets [3]. Emam and Inman [4] reviewed bistable laminates for morphing structures and energy harvesting. Active actuation methods involve integration of smart materials such as piezoelectrics [5] and shape memory alloys [6]. Passive means include thermal [7], mechanical [8], and aerodynamic loading [9].

Regardless of the actuation principle, high-performance smart morphing structures require the ability to sense shape in real time in order to enable shape control. To that end, smart sensors directly embedded as layers in the structure offer a way to measure shapes in a compact and non-intrusive manner. Embedded piezoelectric sensors discussed in the literature tend to address either of two functions: 1) measure smooth and continuous curvature change [10], or 2) measure sharp and discontinuous snap-through events [11], but not both in the same structure. To measure a broad range of possible shapes encountered in morphing bistable composites, both functions are required without negatively affecting morphing performance.

Piezoelectric sensors and actuators are commonly developed using brittle ceramics such as PZT (lead zirconate titanate) and are therefore limited to morphing structures with small curvatures. This limitation is overcome with piezoelectric macro-fiber composites (MFCs) that comprise PZT fibers laminated with interdigitated electrodes [12]. MFCs are flexible and have excellent sensing and actuation properties. They have been used extensively for structural health monitoring, but predominantly in rigid structures [13, 14]. For flexible structures, MFCs are typically integrated as laminae [15] or form the structure

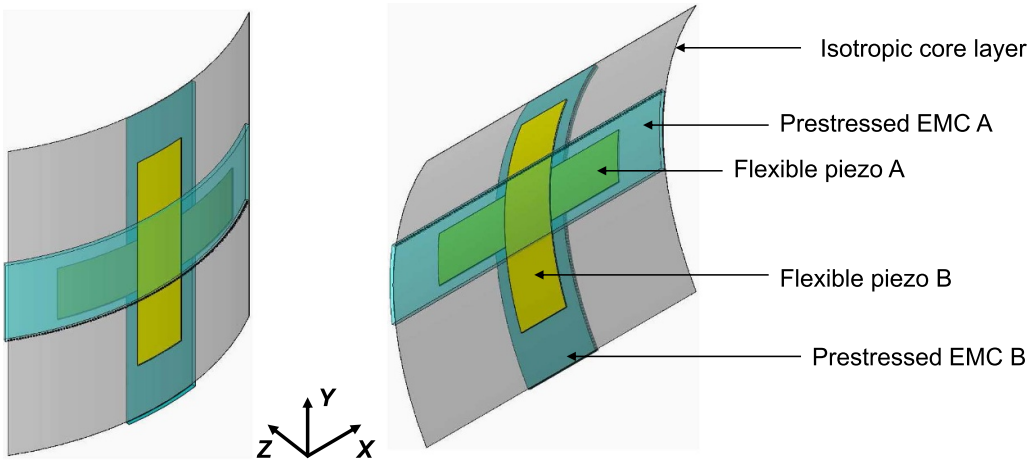

Figure 1. Concept of a self-sensing mechanically-prestressed asymmetric bistable laminate.

themselves [16]. The stiffness of MFCs may not always be negligible relative to the stiffness of the host structure and therefore their mechanical properties should be considered. Sodano *et al* [17] investigated the dynamic-sensing performance of piezoelectric MFC laminae by inducing snap-through in the bistable laminates with an antagonistic MFC pair.

Piezoelectric PVDF (β-crystalline) on the other hand can be realized as thin films or coatings made by electrospinning [18], painting [19], screen printing [20], or 3D printing [21]. Its elastic modulus is approximately a tenth that of MFCs, thus making it non-intrusive for large strain measurements. PVDF sensors are preferred over conventional strain gauges and piezoresistors to track shape changes because they consume minimal power and do not require bulky signal conditioners [22]. Besides PVDF, several organic and inorganic piezoelectric materials [23] are candidate sensor materials for morphing structures.

PVDF films are highly conformable and minimally intrusive on a morphing host structure. They can be miniaturized, patterned, and be fully embedded as wireless sensors [24]. PVDF has been used for vibration detection [25], force and torque sensing [26], and strain sensing [10, 27, 28]. In these applications, a PVDF sensor measures the dynamic response of a structure. There are few implementations of PVDF sensors in bistable structures for self-powered measurement of snap-through events [11].

This paper presents active asymmetric bistable laminates that can sense quasistatic changes in their curvature as well as dynamic snap-through and snap-back responses. To illustrate the approach, rectangular mechanically-prestressed bistable laminates [29] are considered (figure 1) though the methodology is applicable to arbitrary bistable structures. The composite comprises two orthogonally-aligned rectangular PVDF films that are bonded on either face of an initially stress-free core layer. Rectangular strips of prestressed elastomeric matrix composites (EMCs) are laminated on either face of the core such that each EMC is parallel to the PVDF film on the opposite face. The resulting composite has two cylindrical stable shapes that are weakly coupled; each curvature can be tailored by changing only the prestrain in the EMC on the concave or inner face. Although, the PVDF films can be positioned and oriented arbitrarily, the combination of symmetry and orthogonality yields decoupled output signals such that each sensor measures changes in only one cylindrical curvature; the antagonistic sensor measures the snap-through response.

The PVDF-based sensor system developed in this work can measure both static and dynamic responses associated with morphing bistable laminates. PVDF has lower cross sensitivity compared to MFC and is hence more directionally sensitive, making it suitable for detection of specific changes in one curvature while remaining insensitive to the other. When the shapes are weakly coupled, the measured voltage can be directly correlated with changes in the laminate's principal curvature. Due to a linear relationship between the measured voltage and change in curvature, the sensor can be effectively utilized to track the shape of the structure in real time. Further, due to the low power consumption associated with the electronics, the sensor configuration can be simultaneously utilized to harvest energy towards self-powered applications [30].

An analytical modeling approach for the calculation of output voltages associated with shape transition is developed in section 2. In-plane strains and curvatures are calculated for a given set of material and geometric properties using a laminated-plate model. Voltage is calculated based on the charge accumulated due to in-plane strains over the area of the sensor. Experiments developed to characterize the sensors are discussed in section 3. Sensitivity is calculated by correlating the measured voltages with the composite's curvatures tracked using a motion capture system (section 4). The analytical model is validated against the measurements. Model-based analyses are presented in section 5 to explain the effect of prestrain and sensor geometry on the laminate's sensitivity. A comparison between electric and elastic energies is drawn to show how sensor voltages correspond to the mechanical deformation. Conclusions are presented in section 6.

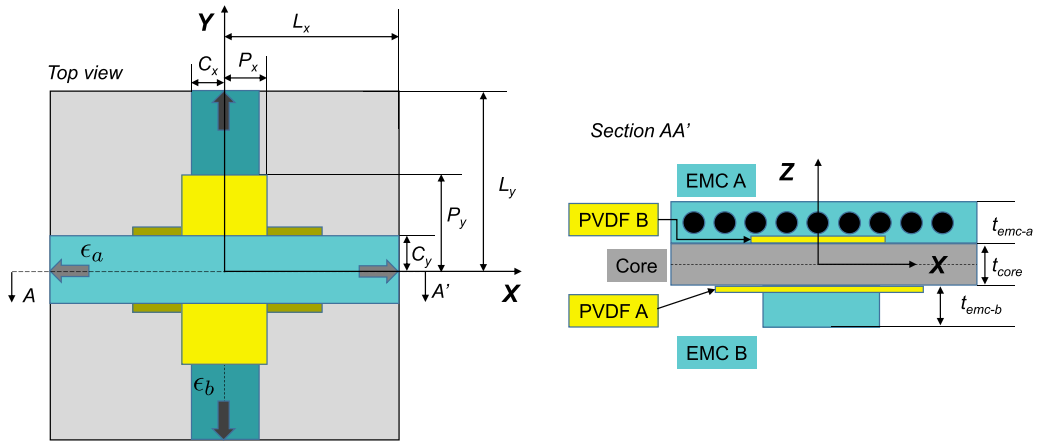

Figure 2. Schematic of a self-sensing bistable laminate for analytical modeling.

2. Analytical model

2.1. Laminate strain formulation

A self-sensing bistable composite is modeled analytically to calculate voltage outputs from the piezoelectric laminae for a given change in curvature. A square laminate with rectangular prestressed EMCs is presented for analysis as illustrated in figure 2. The EMCs are reinforced with fibers along their width to achieve near-zero in-plane Poisson's ratio. Prestrains in EMC A and EMC B, represented by ε_a and ε_b, are applied in the X and Y directions, respectively. The respective weakly coupled cylindrical curvatures of the laminate's geometric centerline are denoted by κ_a and κ_b.

The PVDF layers are rectangular in shape and are poled along their 3-direction. The 1-directions of PVDF A and PVDF B coincide with the directions of prestrains ε_a and ε_b in EMC A and EMC B, respectively. The PVDF layers are assumed to be thin films whose Young's modulus are at least 2 orders of magnitude lower than that of the core layer. Consequently, the material properties of the films are not considered in the calculation of the laminate's stable shapes. Change in stiffness of the PVDF films under an applied strain is assumed to be negligible. Strain in the 3-direction is assumed to be negligible.

The analytical model is formulated in two steps as shown in figure 3. In the first step, composite strains are modeled based on classical laminate theory in conjunction with von Karman's hypothesis; plane stress and plane strain conditions are assumed. In-plane strains and the Z-axis deflection of the geometric mid-plane are described using the following second-degree polynomials under the assumptions of constant curvature and symmetry in the laminate

$$\epsilon_x^0 = c_{00} + c_{20}x^2 + c_{11}xy + c_{02}y^2, \tag{1}$$

$$\epsilon_y^0 = d_{00} + d_{20}x^2 + d_{11}xy + d_{02}y^2, \tag{2}$$

$$w_0 = \frac{1}{2}(px^2 + qxy + ry^2). \tag{3}$$

The deflections of the geometric mid-plane are obtained by integrating the non-linear strain expressions $\epsilon_x^0 = (\partial u_0/\partial x) + 0.5(\partial w_0/\partial x)^2$ and $\epsilon_y^0 = (\partial v_0/\partial y) + 0.5(\partial w_0/\partial y)^2$ with strains described by the polynomials assumed in (1)–(3):

$$u_0 = c_{00}x + f_1 y + \frac{1}{2}\left(c_{11} - \frac{pq}{2}\right)x^2 y + \left(c_{02} - \frac{q^2}{8}\right)xy^2 + \frac{1}{3}\left(c_{20} - \frac{p^2}{2}\right)x^3 + \frac{1}{3}f_3 y^3, \tag{4}$$

$$v_0 = f_1 x + d_{00}y + \frac{1}{2}\left(d_{11} - \frac{qr}{2}\right)xy^2 + \left(d_{20} - \frac{q^2}{8}\right)x^2 y + \frac{1}{3}\left(d_{02} - \frac{r^2}{2}\right)y^3 + \frac{1}{3}f_2 x^3. \tag{5}$$

The total strain energy of the system can be expressed as a function of the strains in the laminate, prestrain in the EMCs, and geometric and material properties of the laminate as:

$$U_T = \int_V \left(U_1 + Q_{12}\epsilon_x\epsilon_y + U_2 + \frac{1}{2}Q_{16}\gamma_{xy}\epsilon_y + \frac{1}{2}Q_{66}\gamma_{xy}^2\right)dV, \tag{6}$$

where

$$\epsilon_x = \epsilon_x^0 - z\frac{\partial^2 w_0}{\partial x^2}, \tag{7}$$

$$\epsilon_y = \epsilon_y^0 - z\frac{\partial^2 w_0}{\partial y^2}, \tag{8}$$

are the in-plane axial strains, and

$$\gamma_{xy} = \frac{\partial u_0}{\partial y} + \frac{\partial v_0}{\partial x} + \frac{\partial w_0}{\partial x}\frac{\partial w_0}{\partial y} - 2z\frac{\partial^2 w_0}{\partial y \partial x} \tag{9}$$

is the in-plane shear strain of the composite. In (6), $\{Q_{ij}\{i,j=1,2,6\}\}$ are the plane stress-reduced stiffness parameters [31] and $U_1 = 0.5(Q_{11}\epsilon_x^2)$, $U_2 = 0.5(Q_{22}\epsilon_y^2)$ are the

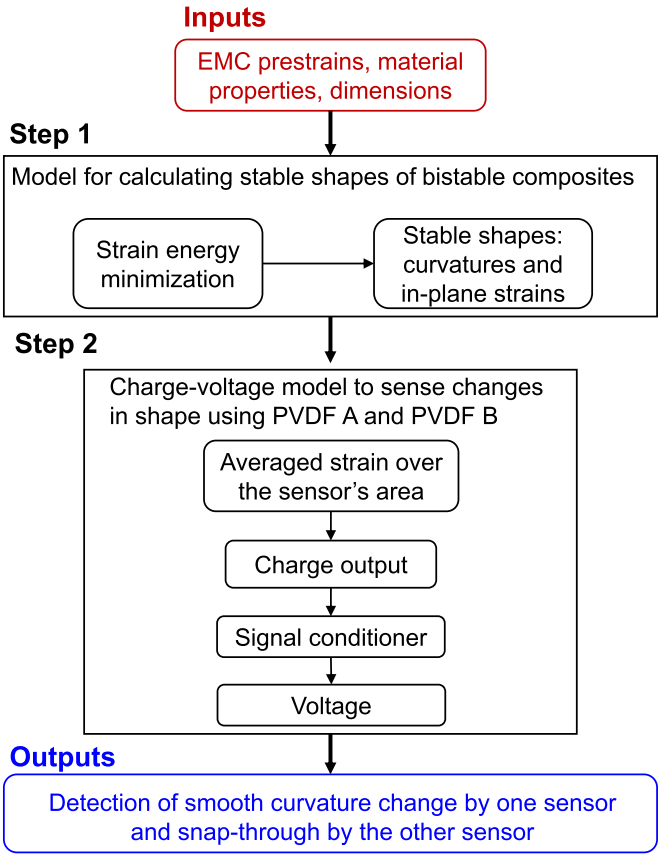

Figure 3. Flowchart of the analytical modeling approach to calculate sensor voltages corresponding to a change in shape.

strain energies in the linearly strained directions in a lamina. In the direction of prestrain, U_1 and U_2 are calculated as the area under the nonlinear stress-strain curve of the EMC [29]. The equilibrium shapes of the laminate are obtained by minimization of (6):

$$\delta U_T = \sum_{i=1}^{14} \frac{\partial U_T}{\partial c_i} \delta c_i = 0, \tag{10}$$

where

$$c_i = \{c_{00}, c_{20}, c_{11}, c_{02}, d_{00}, d_{20}, d_{11}, d_{02}, p, q, r, f_1, f_2, f_3\}. \tag{11}$$

Since (11) is a set of independent variables, each term in (10) must be zero. This yields a set of fourteen non-linear equations; eleven unknown polynomial coefficients $\{c_{00}, c_{20}, c_{11}, c_{02}, d_{00}, d_{20}, d_{11}, d_{02}, p, q, r\}$ from (1)-(3) and three unknown polynomial coefficients $\{f_1, f_2, f_3\}$ from (4) and (5). The set of equations is solved numerically using MATLAB to obtain the strains $(\epsilon_x^0, \epsilon_y^0)$ and curvatures $(\kappa_x^0, \kappa_{xy}^0, \kappa_y^0)$ of the cylindrical laminate's geometric mid-plane. In this paper, κ_x^0, κ_{xy}^0, and κ_y^0, calculated as $-p$,$-q$, and $-r$, are represented for convenience by κ_a, κ_{ab}, and κ_b, respectively. It is noted that (4) and (5) are not required for calculating the charge output of the sensors due to changes in curvature.

The intermediate cylindrical shapes that are associated with snap-through are calculated by applying a range of equal and opposite point forces applied along the X or Y axes. This configuration of forces is chosen to validate the model against tensile tests conducted experimentally to snap the composite.

2.2. Strain-voltage formulation

The spatial distribution of change in strains $\Delta\varepsilon_x(x, y)$ and $\Delta\varepsilon_y(x, y)$ corresponding to a given change in curvature $(\Delta\kappa_a, \Delta\kappa_b)$ is used in step 2 to calculate the average strains over the span of the PVDF layers. Strains in a PVDF layer are calculated as $\epsilon_x = \epsilon_x^0 + z\kappa_a$ and $\epsilon_y = \epsilon_y^0 + z\kappa_b$, where $z\ (= 0.5 \times t_{core})$ is the distance from the PVDF film's contacting surface to the composite's geometric mid-plane. Strain in the PVDF film is assumed to be uniform through its thickness. The charge Q generated due to a change in the average strain over the film's span is calculated as [32]:

$$Q = \frac{A_s}{1 - \nu_{s12}\nu_{s21}} \Big[(d_{31} + \nu_{s21} d_{32}) E_{1s} \Delta\epsilon_{x,avg} + (d_{32} + \nu_{s12} d_{31}) E_{2s} \Delta\epsilon_{y,avg} \Big] \tag{12}$$

where $E_{1s}, E_{2s}, \nu_{s12}$, and ν_{s21} are the in-plane elastic moduli and Poisson's ratios, respectively. The piezoelectric charge coefficients are d_{31} and d_{32}. The area of the sensor is A_s. The subscript s is used to represent sensor parameters.

Charge amplifiers are transimpedance circuits that convert the charge produced by a piezoelectric sensor into measurable voltage. A charge amplifier is typically realized using discrete electronic components designed with an operational amplifier of large gain and a resistive-capacitive $(R_F C_F)$ feedback network [33]. The frequency characteristics of a charge amplifier are those of a band pass filter with its lower cutoff frequency determined by the sensor's impedance Z_S and the feedback impedance Z_F. The upper cutoff frequency is determined by the impedance Z_I comprised of the resistor R_I, sensor capacitance C_S, and the open loop gain A_{OL} of the operational amplifier. In order to facilitate static measurement, the feedback resistance $R_F \to \infty$ such that the time constant of the system $\tau \to \infty$. However, the main drawback of a large time constant charge amplifier is its sensitivity to the input bias currents I_{B-} and I_{B+} that results in a drifting output voltage, contributing to measurement noise and eventually driving the op-amp to saturation. A compact topology for automated drift compensation could be obtained by adding another impedance, equal to the feedback impedance, to the common single-ended charge amplifier and connecting it between the non-inverting op-amp input and the ground as shown in figure 4. The charge amplification stage is followed by a unity gain buffer circuit to provide a low impedance interface to the data acquisition system. Letting $C_S << C_F$, $C_F = C_C$ and $R_F = R_C$, the voltage output from a charge amplifier at low frequencies and compensated for voltage drift error is expressed in the Laplace domain as [32]:

$$V(s) = \left(\frac{sR_F}{sR_F C_F + 1} \right) Q(s) + \left\{ \frac{R_F}{sR_F C_F + 1} (I_{B-} - I_{B+}) \right\}. \tag{13}$$

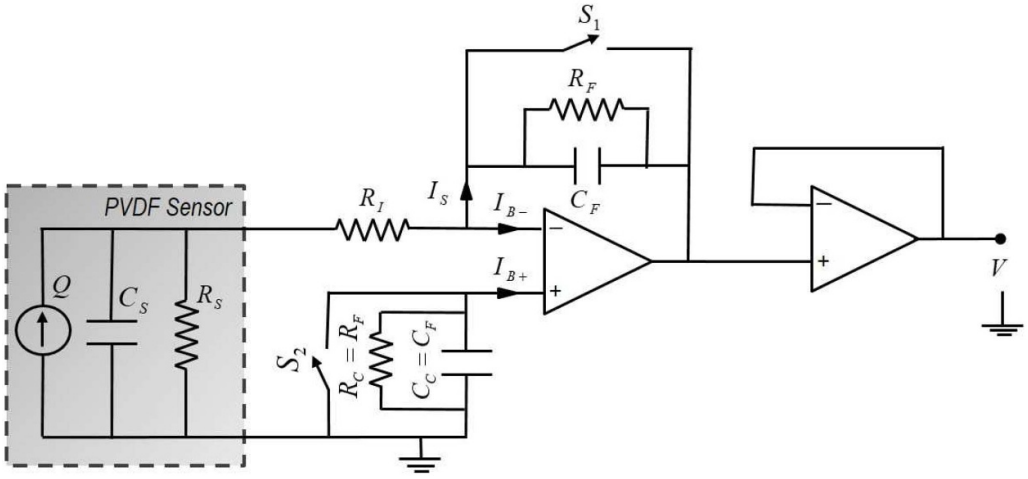

Figure 4. Schematic of the signal conditioner utilized in this application.

For $R_F \to \infty$ and assuming constant capacitance and bias currents, (13) can be rewritten in the time domain as:

$$V(t) = \frac{Q(t)}{C_F} + \underbrace{\frac{t}{C_F}(I_{B-} - I_{B+})}_{e_d} \tag{14}$$

where $S_Q = 1/C_F$ is the gain or calibration factor of the charge amplifier and e_d is the residual drift error. The latter can be minimized by reducing the gain of the charge amplifier and using a low offset current operational amplifier. Thus, the compensated charge amplifier enables a direct readout of the changes generated Q due to the changes in average strains $\Delta\varepsilon_{x,avg}$ and $\Delta\varepsilon_{y,avg}$. Given that each shape is uniquely described by a set of strains and curvatures, the voltages V_a and V_b generated by PVDF A and PVDF B, calculated using the change in strains can be related to the change in curvatures, $\Delta\kappa_a$ and $\Delta\kappa_b$, respectively.

3. Composite fabrication and experimental setup

This section describes the experimental methods developed to characterize the sensitivity of the composite to a given change in shape. The analytical model is then validated using the measured voltages and curvatures.

3.1. Fabrication process

The fabrication of a self-sensing mechanically-prestressed bistable composite [29] includes the integration of sensing layers into the core layer. In the composite demonstrated in figure 5, PVDF films with a thickness of 28 μm sourced from TE Connectivity Ltd. (Measurement Specialities) are laminated on either face of a 76 μm thick spring steel core using flexible silicone adhesive. Prior to lamination, a thin coat of primer is applied to the steel layer to create electrical insulation. Rectangular EMC strips are then stretched to a prestrain of 40% ($\epsilon_a \triangleq \epsilon_b = 0.4$) and bonded simultaneously on either face of the core such that they are orthogonal to the rectangular sensors. A PVDF sensor subjected to plane strain and quasi-static loading conditions exhibits high linearity up to 1000 μstrain [32]. For the chosen EMC prestrain of 0.4, the maximum strain on the PVDF sensor due to the initial curvature is about 350 μstrain. Therefore, the mechanical prestress does not negatively influence its charge sensitivity. The material properties and dimensions of the laminae used in the experiments are listed in table 1. The piezoelectric coupling coefficients (d_{31} and d_{32}) of PVDF are 23 pC/N and 5 pC/N, respectively.

The PVDF laminae are inherently suitable for high-frequency dynamic strain measurements due to their low inertial loading. To enable the quasistatic measurement of smooth changes in the composite's curvature, each PVDF lamina is interfaced with the compensated charge amplifier shown in figure 4. Through this circuit, the time constant is increased to 10^5 seconds with a goal of measuring changes in shape occurring over a time span of 100 seconds with 99% accuracy. To this end, each amplifier is designed to have feedback and compensating capacitances of $C_F = C_C = 100$ nF $\pm$ 1%. The insulating resistances of the capacitors are on the order of 1 TΩ. Ultra-low offset current CMOS operational amplifiers LMC6082 (Texas Instruments) that fit the required design parameters are chosen and operated with a supply voltage of 4.5 V. Input resistances R_I are selected to be 1 MΩ $\pm$ 1% in order to suppress high frequency noise in the system due to the CMOS configuration. The gains of the charge amplifiers are thus calculated as 0.01 mV/pC. Normally-open switches placed across the feedback and compensating capacitors are actuated simultaneously prior to the start of the measurement to reset the circuit by draining any stored charge. The residual error accumulated due to the input bias currents is measured to be as low as 40 μV over 100 seconds.

3.2. Measurement of sensor voltages

Experiments are conducted to measure changes in the composite's shape using the embedded PVDF sensors. Controlled deformations are applied on the structure using a tensile test

Table 1. Dimensions and measured material properties of the laminae used in modeling and experiments.

Lamina	Length (mm)	Width (mm)	Thickness (μm)	E_1 (MPa)	E_2 (MPa)	G_{12} (MPa)	ν_{12}	ν_{21}
Core (steel)	76.2	76.2	76.2	200,000	200,000	78,125	0.28	0.28
PVDF	30	12.2	28	3000	1800	1100	0.35	0.21
EMC	76.2	12.7	1400	0.4	Point-wise	1.2	0	0

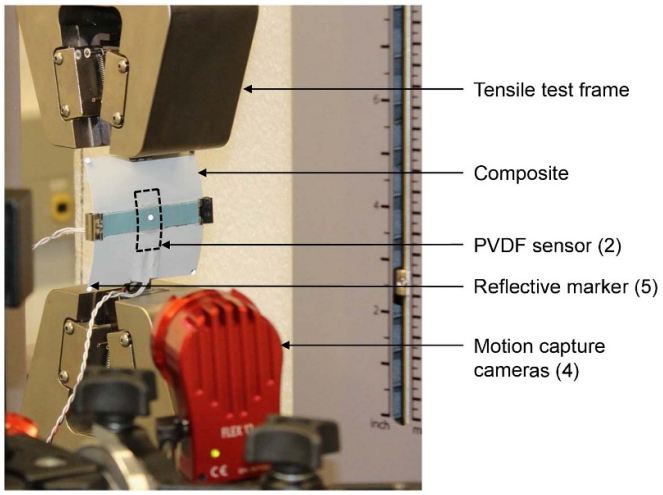

Figure 5. Setup for the measurement of shape change using PVDF sensors and a motion capture system.

frame (figure 5). The composite is hinged at the mid-points of its straight edges in one stable shape and flattened at a rate of 0.1 mm/s until it snaps into the next stable shape. A 3D motion capture system is used to track reflective markers placed at the center and the vertices of the composite. The cameras are synchronized with the load frame and the sensor circuits to sample at 100 frames per second. Composite shape is reconstructed using the marker coordinates under the assumption of constant curvature. The voltages measured by the PVDF sensors are recorded using a data acquisition system (National Instruments) and LabView.

4. Model validation and discussion

The experimental results shown in this section correspond to a transition in curvature from κ_a to κ_b; results in the case of snap-back would be similar since the curvatures in the chosen composite are equal. Prior to snap-through, the curved composite has sensor A on the outer face and sensor B on the inner face. The corresponding voltage signals V_a and V_b from the PVDF sensors are shown in figures 6(a) and (b), respectively. In the absence of a charge amplifier, both sensors detect only the snap-through event in the form of a sharp transient response. Inclusion of the large time constant compensated charge amplifier results in a linear increase in the voltage magnitude of sensor *A* up to snap-through. The voltage remains in steady state post-snap through. Sensor B, on the other hand, detects only the snap-through event through a step change from zero to a finite voltage. The transient snap-through responses in both sensors are filtered by the charge amplifier due to the large C_F/C_S ratio, thus enabling the tracking of smooth and discontinuous shape transitions. In the absence of the charge amplifier, sensor B produces a larger instantaneous voltage response compared to sensor A. Such a response is attributed to a greater strain in sensor B during the snap-through from κ_a to κ_b. On the other hand, with the inclusion of the compensated charge amplifier, the steady state voltage magnitudes post snap-through are the same in both sensors. Since the charge amplifier is reset prior to the measurement, the voltage output directly corresponds to the change in average strain of the sensor. In the context of self-powered sensing, figure 6 suggests that for a shape transition from κ_a to κ_b, any energy harvesting mechanism should be coupled to PVDF B.

Figures 7(a) and (b) show a strong correlation between voltages recorded by each sensor over a given timescale and the curvatures tracked by the motion capture system. Such a response is attributed to the linear strain response of the piezolelectric laminae. Within the morphing structure, PVDF A tracks κ_a and PVDF B tracks κ_b. Voltage in PVDF A is negative and decreases with a decrease in κ_a because the layer experiences compressive strain in the 1-direction as the laminate is flattened (figure 7(a)). Beyond snap through, PVDF A remains physically flat in the 1-direction and develops curvature in the 2-direction. This is indicated by the stable voltage output post snap-through. Without the large time constant charge amplifier, the signal will decay to zero. The deviation from linearity in V_a towards a higher slope, observed just prior to snap-through, can be explained by a downward shift in the post snap-through voltage due to compressive strain in the 2-direction. The shift or offset in the 2-direction is evident in the pre-snap-through response of PVDF B (figure 7(b)). The snap-through frequencies measured by PVDF A and PVDF B, and the motion capture system are 33, 33, and 36 Hz, respectively.

The relationship between the generated voltage and the change in curvature is defined in terms of the sensitivities ($\lambda_{ij}, i = \{a, b\}$) of PVDF A and PVDF B as:

$$\begin{Bmatrix} V_a \\ V_b \end{Bmatrix} = \underbrace{\begin{bmatrix} \lambda_{aa} & \lambda_{ab} \\ \lambda_{ba} & \lambda_{bb} \end{bmatrix}}_{\mathbf{\Lambda}} \begin{Bmatrix} \Delta\kappa_a \\ \Delta\kappa_b \end{Bmatrix}, \tag{15}$$

where $\{\lambda_{aa}, \lambda_{bb}\}$ and $\{\lambda_{ab}, \lambda_{ba}\}$ are the laminate's direct and cross sensitivities, respectively. The voltage-curvature response of the sensing laminae obtained from measurements and analytical modeling is plotted in figure 8 and the sensitivities are tabulated in table 2. Direct sensitivity (λ_{ii}) is associated with the sensor that undergoes smooth curvature change, whereas cross sensitivity (λ_{ij}) of the same sensor is

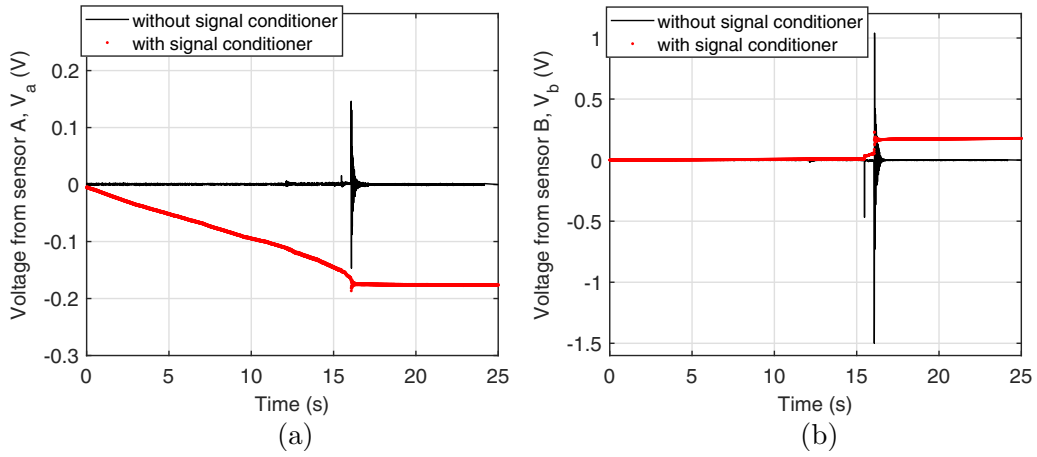

Figure 6. Quasistatic and dynamic voltages measured during shape transition from κ_a to κ_b in (a) PVDF A and (b) PVDF B.

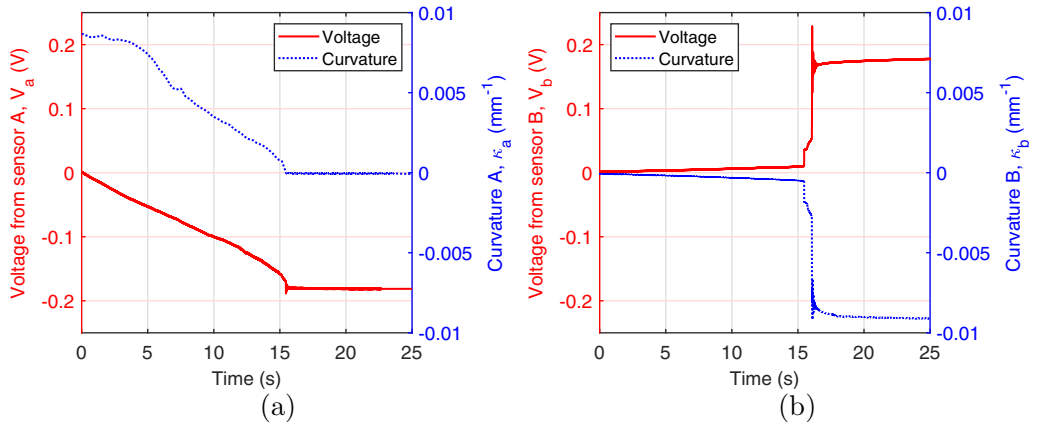

Figure 7. Correlation between measured voltages and curvature change represented as: (a) V_a from PVDF A vs. κ_a and (b) V_b from PVDF B vs. κ_b.

Table 2. Measured and modeled sensitivities of a self-sensing bistable laminate. Units are V-mm. The average value of λ_{aa} from the non-linear $V_a - \Delta\kappa_a$ curve, is listed.

Method	λ_{aa}	λ_{ab}	λ_{ba}	λ_{bb}
Experiment	−15.33	2.56	0.915	−19.4
Model, lower limit of $Y_s = 2$ (GPa)	−12.11	4.53	4.53	−12.11
Model, upper limit of $Y_s = 4$ (GPa)	−23.81	9.06	9.06	−23.81

associated with snap-through and minimal curvature change. For example, when snapping from κ_a to κ_b, λ_{aa} is larger than λ_{bb}. Due to weak coupling between the shapes, there is asymmetry in the sensitivities during both shape transitions, i.e. the cross sensitivities are always lower than their direct sensitivities. Given the variability in the processing of PVDF laminae, the sensitivities are calculated using the analytical model for Young's moduli ranging from 2 to 4 GPa (range prescribed by the manufacturer).

The direct sensitivities lie within the range of the model-calculated values. The deviation of the calculated cross sensitivities from the measured values can be attributed to the assumption of constant curvature in the analytical model. Mechanically-prestressed bistable laminates with cylindrical shapes have been shown to exhibit flat regions across the width of the EMCs [29]; the unidirectional fibers in the width direction restrict curvature. Given that the PVDF laminae have similar width as the EMCs, curvature of the PVDF sensor in the 2-direction deviates from the model-calculated value, thereby resulting in lower cross-sensitivity. For both sensors, the ratio of the model-calculated direct sensitivity to cross sensitivity is calculated to be 2.65 for an average Y_s of 3 GPa. Due to the linear behavior of the sensor and the asymmetry, the measured voltages and sensitivities directly relate to the principal curvatures. Therefore, at any given instant, the shape of the composite can be completely described from the set of values comprised of $\{V_a, V_b, \lambda_{aa}, \lambda_{ab}\}$. In a bistable composite with unequal stable curvatures, it is necessary to know V_a, V_b, and the curvature sensitivity matrix $\mathbf{\Lambda}$ to completely describe the shape in real-time.

5. Model-based Analysis

The relationships between sensor geometry, curvatures, and EMC prestrains are studied to identify and understand the

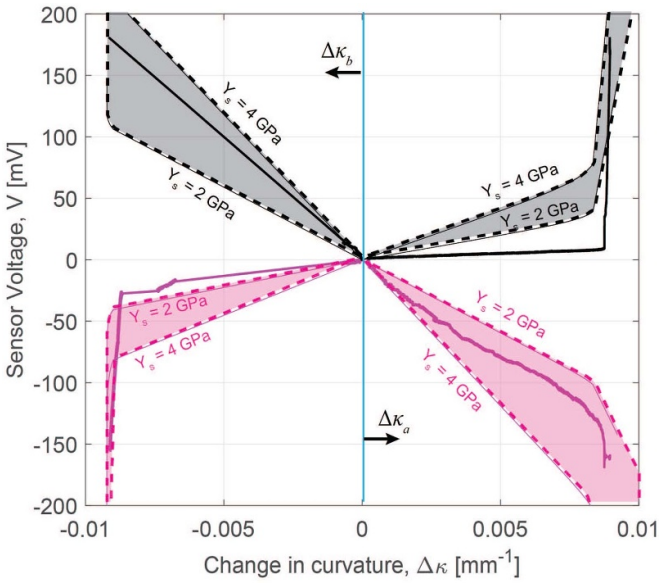

Figure 8. Voltages from PVDF A (magenta) and PVDF B (black) vs. curvature obtained from experiments (solid lines) and modeling (dashed lines).

design space of self-sensing bistable laminates. Elastic and electrical energies are calculated for various curvatures and prestrains towards a quantitative description of the structure. The material and geometric properties used in these parametric studies are the same as listed in table 1. EMC prestrains ε_a and ε_b of 0.4 are maintained in the analyses unless otherwise mentioned.

5.1. Effect of EMC prestrain on sensitivity

Further analysis is conducted by calculating the sensitivities of the laminate for prestrain in EMC A ε_a ranging from 0.2 to 0.6 with ε_b constant at 0.4. The prestrain range is chosen such that it falls within the domain of bistability of the laminate. Percentage change in sensitivities relative to a configuration with equal prestrains ($\epsilon_a \triangleq \epsilon_b = 0.4$) is calculated for the cylindrical stable shapes described by κ_a and κ_b in figures 9(a) and (b), respectively. The direct sensitivity λ_{bb} is minimally affected by changes in ε_a due to a weak coupling between shapes that renders κ_b to be independent of ε_a. The direct sensitivities represent smooth curvature sensing due to a weak shape coupling and a smaller d_{32} compared to the d_{31} coefficient. However, the cross sensitivities exhibit strong dependence on the prestrain in the EMCs because the overall change in curvature ($|\kappa_a| + |\kappa_b|$) changes with change in ε_a. It is noted that the direct and cross sensitivities represent the limiting cases of curvature sensitivities for a given laminate.

5.2. Effect of sensor geometry on sensitivity

The PVDF laminae generate charge proportional to the change in average in-plane strains on their surface. As a result, the measured voltage depends not only on the dimensions of the layers, but also on their spatial position and shape. Figures 10(a) and (b) show the strain profiles on the outer surface ($z = 0.5 \times t_{core}$) on a laminate with curvature κ_a. Strain ε_y is calculated to be two orders of magnitude lower than ε_x. Flattening of the laminate considered results in a change in ε_x of 348 μstrain.

The PVDF curvature sensors developed in this work operate in charge mode in contrast to piezoelectric devices such as energy harvesters and vibration sensors that typically operate in voltage mode. Due to the low permittivity of PVDF, the effect of the sensor's capacitance is negligible and sensitivity depends only on its area. Figure 11 shows the sensitivity as a function of the area and aspect ratio of a rectangular lamina. Sensitivity is maximum at an aspect ratio of 1 and an area that corresponds to the sensor spanning the entire core layer. Due to the small in-plane variations on the laminate's surface, sensitivity is almost unaffected by the spatial position of the sensing layer relative to the core layer. For a given area, sensitivity decreases with an increase in aspect ratio (beyond 1) but has a finite value so long as the area is finite. These results suggest that PVDF sensors can be embedded as fibers or printed as lines for robust integration of the sensing system. Curvature sensitivities $\mathbf{\Lambda}$ of the laminae are maximum when the 1-directions are aligned with the principal curvatures of the laminate as shown in figure 2; in such a configuration the PVDF laminae are orthogonal. A shift from orthogonality results in a decrease in $\mathbf{\Lambda}$ since $d_{32} < d_{31}$ necessitating recalibration of the curvature cross-sensitivity of the sensors with change in prestrain.

5.3. Calculation of elastic and electrical energies

The elastic and electrical energies are studied to investigate the energy harvesting capacity of the structure. The analysis can be further extended towards health monitoring applications. Figure 12(a) shows the change in elastic energies for different prestrains ε_a with ε_b kept constant at 0.4. In the case of equal prestrains, the energy-curvature profiles are symmetric with respect to the flat shape. Increasing the prestrains results in an increase in the stored elastic energy when transitioning from higher to lower curvature. The snap-through actuation energy of the structure corresponds to the peak of the elastic energy profile. Also, the energy peak is skewed towards the shape with the larger prestrain (κ_a in figure 12(a)).

The piezoelectric energy E_p can be calculated from the sensors' voltage as [34] :

$$E_p = \frac{1}{2}\frac{Q^2}{C_S} = \frac{V^2}{2S_Q^2 C_S} \tag{16}$$

Figure 12(b) shows the cumulative electrical energies generated by the sensors when the laminate switches from one stable κ_a to κ_b. The energy generated by PVDF A increases with increase in ε_a, in accordance with the increase in elastic energy, due to higher initial curvature. The effect of changing ε_a on the energy in PVDF B is not significant. A sharp discontinuity is observed when the laminate crosses the flat shape ($\kappa = 0$) due to the switching between direct and cross sensitivities. Unlike the strain energy

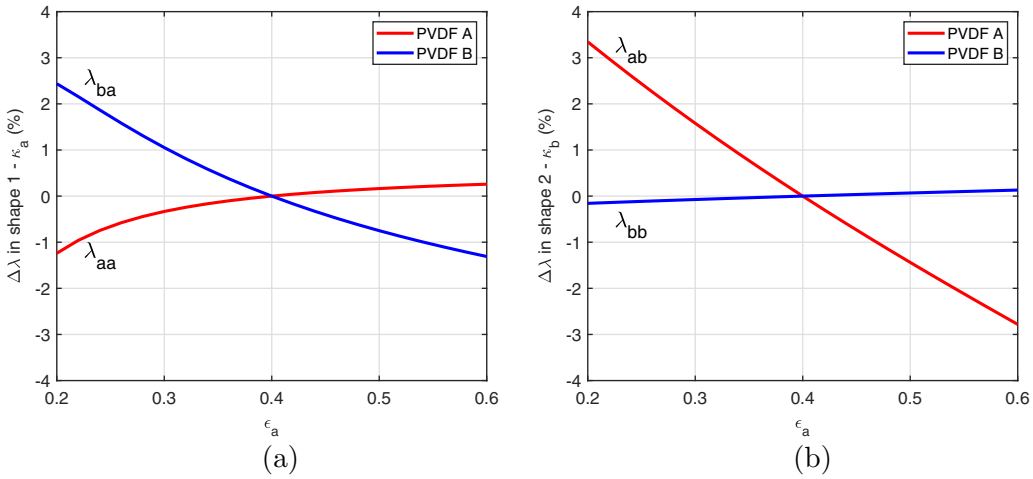

Figure 9. Percentage change in curvature sensitivity due to a change in EMC prestrain ε_a as seen in the shape represented by (a) ε_a and (b) ε_b.

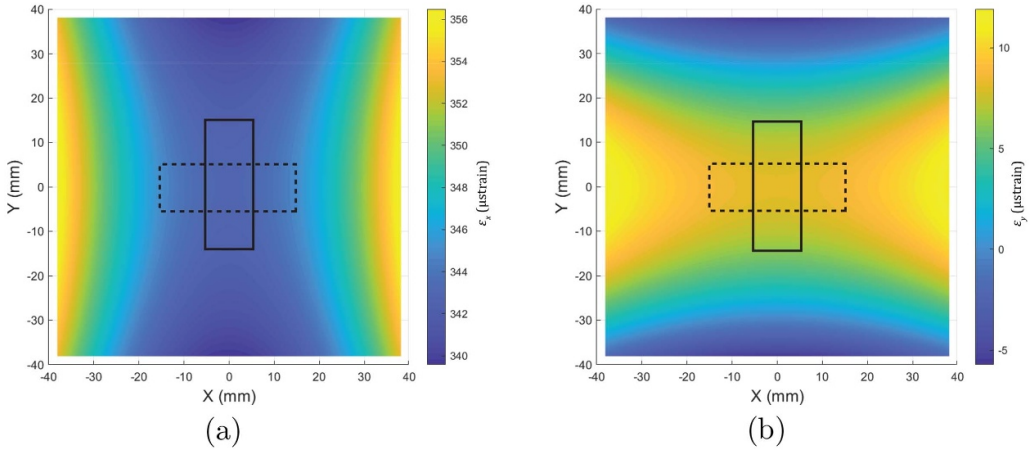

Figure 10. Strain profiles (a) ε_x and (b) ε_y of the laminate corresponding to a stable curvature κ_a ($\varepsilon_a \triangleq \varepsilon_b = 0.4$). Solid and dashed lines represent the outer PVDF A and inner PVDF B laminae, respectively.

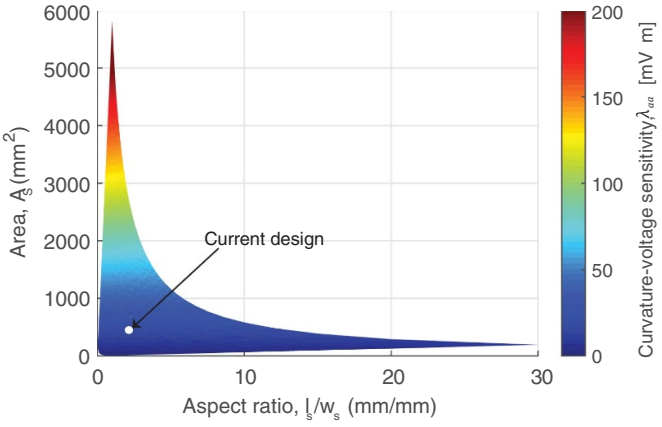

Figure 11. Curvature sensitivity as a function of a sensing layer's area and aspect ratio.

profiles, the snap-through curvatures cannot be identified from the electrical energy profiles. This is due to the fact that the mechanics of the PVDF layer are not considered in the model. Nevertheless, the electrical energy at zero curvature can be effectively utilized to monitor the actuation requirements.

The electrical energy plot also provides insights into the maximum energy that can be harvested from a single shape transition. The total electrical energies (and voltages) generated by the sensors for a complete shape transition are equal for a laminate with equal prestrains ($\varepsilon_a = \varepsilon_b$); this case is represented by the closed loop in figure12(b). However, deviation or deterioration in shapes, represented using a change in prestrains, can be tracked and quantified using the electrical energies in both sensors. For example, when $\varepsilon_a = 0.6$ and $\varepsilon_b = 0.4$, PVDF A generates 33% higher energy compared to PVDF B. However, increasing prestrain beyond 1 (100%) has a marginal benefit in terms of actuation and energy harvesting performance due to the high shear stress at the interface [35]. Alternatively, the curvature can be amplified for a given prestress by decreasing the elastic modulus or thickness of the core layer. But reducing the thickness or elastic modulus of the host structure can adversely affect the strain transfer and thereby the curvature sensitivity of the PVDF sensor [36]. Finally, the electrical energy represents the energy harvesting capacity of the structure.

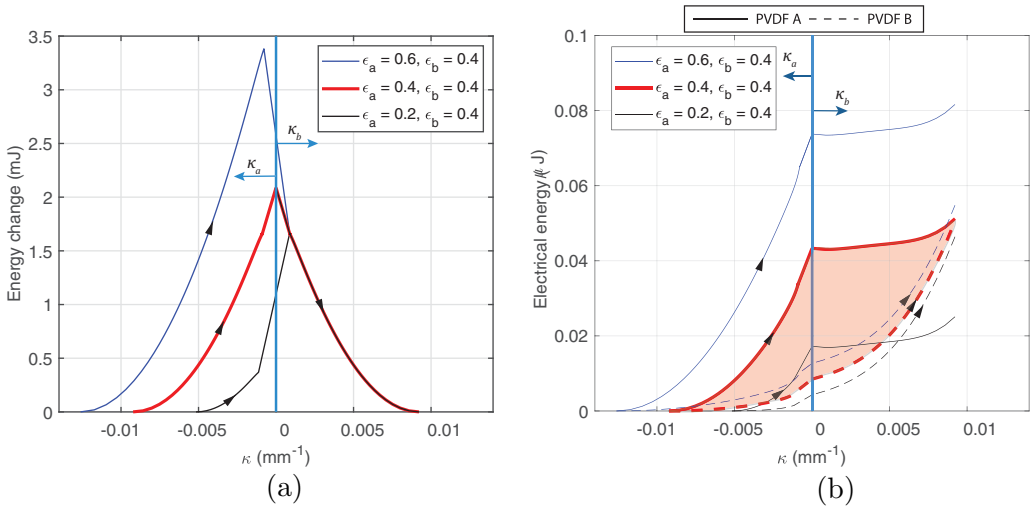

Figure 12. (a) Elastic energy corresponding to shape transition and (b) electrical energy generated by the PVDF sensors over the transition from a stable κ_a to κ_b. Prestrain ε_b is maintained constant at 0.4.

6. Conclusions

This paper presented an active asymmetric bistable laminate comprised of piezoelectric PVDF films that can sense near static changes in its curvature as well as the dynamic snap-through and snap-back responses. A method for the fabrication of the active bistable laminate is described. A large time constant compensated charge amplifier is interfaced with the PVDF sensors to enable a direct readout of shape change and dynamic snap-through. An analytical model that relates the change in shape to voltage output by the sensors is presented. The experimental results suggest a strong correlation between the voltages recorded by each sensor and the curvatures tracked by the motion capture system. The weakly coupled shapes of the laminate and the lower cross sensitivity of PVDF enable direct measurement of the principal curvatures. The analytical model successfully captures the measured values of curvature sensitivities. Due to the linearity between the change in curvature and voltages, the shape of the composite can be tracked in real-time from the measured parameters. The model-based analyses established the effect of EMC prestrain, sensor geometry, and position on curvature sensitivity. It is observed that the EMC prestrain has a stronger effect on cross sensitivities than direct sensitivities of the curvature sensor. Further, due to positional invariance, the sensors can be patterned and embedded as fibers for robust integration of the sensing system. The inherent ability of the piezoelectric sensors to generate electrical energy in response to change in elastic energy can be employed to monitor the structural condition of the laminate and power wireless sensor networks.

Acknowledgments

Financial support was provided by the member organizations of the Smart Vehicle Concepts Center, a Phase III National Science Foundation Industry-University Cooperative Research Center (www.SmartVehicleCenter.org) under grant NSF IIP 1738723.

ORCID iDs

V S C Chillara https://orcid.org/0000-0001-6651-3763
M J Dapino https://orcid.org/0000-0003-4888-1903

References

[1] Daynes S, Weaver P M and Trevarthen J A 2011 A morphing composite air inlet with multiple stable shapes *J. Intell. Mater. Syst. Struct.* **22** 961–73
[2] Spiteri L, Daynes S and Watkins S 2015 Design of a morphing Bi-Stable composite air intake *SAE Technical Paper* https://doi.org/10.4271/2015-01-0066
[3] Gatto A, Mattioni F and Friswell M I 2009 Experimental investigation of bistable winglets to enhance aircraft wing lift takeoff capability *J. Aircr.* **46** 647–55
[4] Emam S A and Inman D J 2015 A review on bistable composite laminates for morphing and energy harvesting *Appl. Mech. Rev.* **67** 060803
[5] Gude M, Hufenbach W and Kirvel C 2011 Piezoelectrically driven morphing structures based on bistable unsymmetric laminates *Compos. Struct.* **93** 377–82
[6] Kim H A, Betts D N, Salo A T and Bowen C R 2010 Shape memory alloy - piezoelectric active structures for reversible actuation of bistable composites *Am. Inst. Aeronaut. Astronaut.* **48** 1265–8
[7] Eckstein E, Pirrera A and Weaver P M 2014 Multi-mode morphing using initially curved composite plates *Compos. Struct.* **109** 240–5
[8] Lachenal X, Daynes S and Weaver P M 2013 A zero torsional stiffness twist morphing blade as a wind turbine load alleviation device *Smart Mater. Struct.* **22** 065016
[9] Arena G, Groh R M J, Theunissen R, Weaver P M and Pirrera A 2018 Design and testing of a passively adaptive inlet *Smart Mater. Struct.* **27** 085019
[10] Shapiro Y, Kósa G and Wolf A 2014 Shape tracking of planar Hyper-Flexible beams via embedded PVDF deflection sensors *IEEE/ASME Trans. Mechatron.* **19** 1260–7

[11] Lajnef N, Burgueño R, Chakrabartty S and Borchani W 2013 Self-Powered sensing system for the monitoring of Quasi-Static structural response *ASME 2013th Conf. on Smart Materials, Adaptive Structures and Intelligent Systems* American Society of Mechanical Engineers p V002T07A022–V002T07A022

[12] Wilkie W K, Bryant R G, High J W, Fox R L, Hellbaum R F, Jalink A, Little B D and Mirick P H 2000 Low-cost piezocomposite actuator for structural control applications *SPIE's 7th Annual Int. Symp. on Smart Structures and Materials* Int. Society for Optics and Photonics pp 323–34

[13] Brunner A J, Birchmeier M, Melnykowycz M M and Barbezat M 2009 Piezoelectric fiber composites as sensor elements for structural health monitoring and adaptive material systems *J. Intell. Mater. Syst. Struct.* **20** 1045–55

[14] Park S, Inman D J and Yun C-B 2008 An outlier analysis of MFC-based impedance sensing data for wireless structural health monitoring of railroad tracks *Engineering Structures* **30** 2792–9

[15] Hufenbach W, Gude M and Czulak A 2006 Actor-initiated snap-through of unsymmetric composites with multiple deformation states *J. Mater. Process. Technol.* **175** 225–30

[16] Lee A J, Moosavian A and Inman D J 2017 A piezoelectrically generated bistable laminate for morphing *Mater. Lett.* **190** 123–6

[17] Sodano H A, Park G and Inman D J 2004 An investigation into the performance of macro-fiber composites for sensing and structural vibration applications *Mech. Syst. Signal Process.* **18** 683–97

[18] Liu Z H, Pan C T, Su C Y, Lin L W, Chen Y J and Tsai J S 2014 A flexible sensing device based on a PVDF/MWCNT composite nanofiber array with an interdigital electrode *Sensors Actuators* A **211** 78–88

[19] Hale J M, White J R, Stephenson R and Liu F 2005 Development of piezoelectric paint thick-film vibration sensors *Proc. Inst. Mech. Engineers* C **219** 1–9

[20] Emamian S, Avuthu S G R, Narakathu B B, Eshkeiti A, Chlaihawi A A, Bazuin B J, Joyce M K and Atashbar M Z 2015 Fully printed and flexible piezoelectric based touch sensitive skin *2015 Ieee Sensors* pp 1–4

[21] Kim H, Torres F, Wu Y, Villagran D, Lin Y and Tseng T-L 2017 Integrated 3D printing and corona poling process of PVDF piezoelectric films for pressure sensor application *Smart Mater. Struct.* **26** 085027

[22] Harrison J S and Ounaies Z 2002 Piezoelectric polymers *Encyclopedia of Polymer Science and Technology* (Chichester: Wiley) **3**

[23] Dagdeviren C, Joe P, Tuzman O L, Park K-I, Lee K J, Shi Y, Huang Y and Rogers J A 2016 Recent progress in flexible and stretchable piezoelectric devices for mechanical energy harvesting, sensing and actuation *Extreme Mech. Lett.* **9** 269–81

[24] Gu H, Zhao Y and Wang M L 2005 A wireless smart PVDF sensor for structural health monitoring *Struct. Control Health Monitor.* **12** 329–43

[25] Park G, Ruggiero E and Inman D J 2002 testing of inflatable structures using smart materials *Smart Mater. Struct.* **11** 147

[26] Ma L, Melkote S N and Castle J B 2014 PVDF sensor-based monitoring of milling torque *Int. J. Adv. Manuf. Technol.* **70** 1603–14

[27] Ling M, Cao J, Li Q and Zhuang J 2018 Design, pseudostatic model and PVDF-Based motion sensing of a Piezo-Actuated XYZ flexure manipulator *IEEE/ASME Trans. Mechatron.* **23** 2837–48

[28] Shapiro Y, Wolf A and Kósa G 2012 Compliant bi-bellows actuator with PVDF force-shape sensing *2012 4th IEEE RAS EMBS Int. Conf. on Biomedical Robotics and Biomechatronics (BioRob)* pp 1602–6

[29] Chillara V S C and Dapino M J 2017 Mechanically-prestressed bistable composite laminates with weakly coupled equilibrium shapes *Composites* B **111** 251–60

[30] Maruccio C, Quaranta G, De Lorenzis L and Monti G 2016 Energy harvesting from electrospun piezoelectric nanofibers for structural health monitoring of a cable-stayed bridge *Smart Mater. Struct.* **25** 085040

[31] Reddy J N 2006 *Theory and Analysis of Elastic Plates and Shells* (Boca Raton, FL : CRC press)

[32] Ramanathan A K, Headings L M and Dapino M J 2020 Near static strain measurement with piezoelectric films *Sensors Actuators* A **301** 111654

[33] Gautschi G 2002 *Piezoelectric Sensorics* (Berlin: Springer) pp 73–91

[34] Leo D J 2007 *Engineering Analysis of Smart Material Systems* (New York: Wiley)

[35] Chillara V S C and Dapino M J 2018 Stability considerations and actuation requirements in bistable laminated composites *Compos. Struct.* **184** 1062–70

[36] Taewoo H, Zhang J X J and Nanshu L 2016 Thickness ratio and d 33 effects on flexible piezoelectric unimorph energy conversion *Smart Mater. Struct.* **25** 035037